High harmonic fast wave heating efficiency enhancement and current drive at longer wavelength on the National Spherical Torus Experiment[a)]

J. Hosea,[1,b)] R. E. Bell,[1] B. P. LeBlanc,[1] C. K. Phillips,[1] G. Taylor,[1] E. Valeo,[1] J. R. Wilson,[1] E. F. Jaeger,[2] P. M. Ryan,[2] J. Wilgen,[2] H. Yuh,[3] F. Levinton,[3] S. Sabbagh,[4] K. Tritz,[5] J. Parker,[6] P. T. Bonoli,[7] R. Harvey,[8] and NSTX Team

[1]*Princeton Plasma Physics Laboratory, Princeton University, Princeton, New Jersey 08540, USA*
[2]*Oak Ridge National Laboratory, Oak Ridge, Tennessee 37831, USA*
[3]*Nova Photon Incorporated, Princeton, New Jersey 08543, USA*
[4]*Columbia University, New York, New York 10025, USA*
[5]*Johns Hopkins University, Baltimore, Maryland 21218, USA*
[6]*Cornell University, Ithaca, New York 14853, USA*
[7]*Plasma Science and Fusion Center, Massachusetts Institute of Technology, Cambridge, Massachusetts 02139, USA*
[8]*CompX, Del Mar, California 92014, USA*

(Received 9 November 2007; accepted 2 January 2008; published online 14 February 2008)

High harmonic fast wave heating and current drive (CD) are being developed on the National Spherical Torus Experiment [M. Ono *et al.*, Nucl. Fusion **41**, 1435 (2001)] for supporting startup and sustainment of the spherical torus plasma. Considerable enhancement of the core heating efficiency (η) from 44% to 65% has been obtained for CD phasing of the antenna (strap-to-strap $\phi=-90°$, $k_\phi=-8$ m^{-1}) by increasing the magnetic field from 4.5 to 5.5 kG. This increase in efficiency is strongly correlated to moving the location of the onset density for perpendicular fast wave propagation ($n_{\text{onset}} \propto B \times k_\parallel^2/\omega$) away from the antenna face and wall, and hence reducing the propagating surface wave fields. Radio frequency (RF) waves propagating close to the wall at lower B and $k_\parallel$ can enhance power losses from both the parametric decay instability (PDI) and wave dissipation in sheaths and structures around the machine. The improved efficiency found here is attributed to a reduction in the latter, as PDI losses are little changed at the higher magnetic field. Under these conditions of higher coupling efficiency, initial measurements of localized CD effects have been made and compared with advanced RF code simulations. © *2008 American Institute of Physics*. [DOI: 10.1063/1.2837051]

I. INTRODUCTION

High harmonic fast wave (HHFW) heating and current drive (CD) are being explored on the National Spherical Torus Experiment (NSTX) (Ref. 1) to assist plasma ramp-up in the absence of ohmic inductive drive and to help sustain the plasma for long discharge times. NSTX is a low magnetic field device ($B_\phi \leqslant 5.5$ kG) for which the 30 MHz HHFW radio frequency (RF) system[2] operates at a relatively high ion cyclotron harmonic: ~ 8 m^{-1} for deuterium/helium on axis. Success in applying HHFW heating and/or CD on NSTX could help to establish the viability of the spherical torus (ST) concept as a long-pulse, or even steady-state, component test facility (CTF) at higher magnetic field, where efficient HHFW coupling could prove to be more readily obtained. The experimental HHFW studies on NSTX are focused first on establishing efficient heating at launched wavelengths desirable for heating and CD, and then on optimizing the CD that can be achieved. It is essential to understand the power loss and CD processes, in order to optimize the heating and CD efficiencies, and to ultimately extrapolate both to the conditions of the higher magnetic field CTF device.

The general problem of optimizing the RF power coupled to the core of a toroidal plasma device has long been of interest because it is an essential prerequisite for efficient RF heating and CD. Some time ago, it had been observed on several tokamaks that the heating efficiency was greater for out-of-phase operation between adjacent current straps of the antennas than for in-phase operation[3,4] and that in-phase operation produces considerably more impurities.[5,6] Many mechanisms may have contributed to this observed behavior, including properties of near field sheath bombardment of the antenna,[7,8] parametric decay instability (PDI) heating,[9] and fast wave damping in the edge plasma region due to collisions and sheaths. For the HHFW regime on NSTX, the RF waves are launched into NSTX at a frequency of 30 MHz with a large 12 strap antenna array that spans $\sim 90°$ toroidally around the outside of the torus. By feeding this antenna with six decoupled sources, any strap-to-strap phase between 0° and 180° may be chosen for the first six straps, with the next set of six straps following these with a 180° phase shift. As a consequence, very good toroidal spectral definition[2] (especially for $\pm 90°$ and $\pm 30°$ between adjacent antenna straps) is obtained, so that it is possible to determine the coupling properties as a function of launched toroidal wavelength with considerable precision. This allows a separation of PDI and propagating fast wave effects and a demonstra-

[a)]Paper JI1 5, Bull. Am. Phys. Soc. **52**, 142 (2007).
[b)]Invited speaker.

tion of the importance of separating the propagation region sufficiently from the antenna/wall.

A major objective for the HHFW program on NSTX is to heat the electrons and drive current simultaneously. For this purpose the antenna was designed to support a very peaked directed spectrum at $k_\phi = -8\ \mathrm{m}^{-1}$, which corresponds to −90° phasing between adjacent current straps and propagation in the direction to provide co-CD. In order to quantify the amount of RF power deposited in the electrons and ions of the core plasma, RF power pulses are applied and the stored energy (W_e) for the electrons and the total plasma stored energy (W_T) are fitted with an exponential rise/fall function:[10]

$$W(t) = W_0 - (W_0 - W_F) \times (1 - e^{-t/\tau}), \tag{1}$$

where W_0 is the energy at the beginning of the pulse and W_F is the asymptotic value that would be obtained without further pulsing. The total stored energy W_T is obtained from the magnetic equilibrium code EFIT,[11] and the electron stored energy W_e is obtained by integrating Thomson scattering kinetic electron pressure $P_e(r)$ over the EFIT magnetic field surface volumes. The power into electrons and into the total plasma is then equated to $P_e = \Delta W_{eF}/\tau_e$ and $P_T = \Delta W_{TF}/\tau_T$, respectively, for each RF power pulse. Finally, the core electron and plasma heating efficiencies are defined as $\eta_e = P_e/\Delta P_{\mathrm{RF}}$ and $\eta_T = P_T/\Delta P_{\mathrm{RF}}$, where ΔP_{RF} is the increment in RF power at the pulse.

Earlier results obtained at a toroidal magnetic field of $B_\phi = 4.5$ kG showed that Eq. (1) fits the heating data well.[10] However, it was found that the heating efficiencies for $k_\phi = -8\ \mathrm{m}^{-1}$ (−90° co-CD phasing) were about half of the values at $k_\phi = 14\ \mathrm{m}^{-1}$ (180° heating phasing), with $\eta_e(\%) = 48$ and 22, and $\eta_T(\%) = 68$ and 44 for $k = 14\ \mathrm{m}^{-1}$ and $-8\ \mathrm{m}^{-1}$, respectively, under similar plasma conditions. The PDI was observed with spectral measurements of probe and edge reflectometry signals, and associated edge ion heating was observed with a spectroscopic edge rotation diagnostic (ERD).[12] However, the power loss that could be attributed to this edge ion heating was comparable for the two cases—the maximum power loss was ~16% and 23% for $k_\phi = 14\ \mathrm{m}^{-1}$ and $-8\ \mathrm{m}^{-1}$, respectively. Therefore, this edge ion heating could not account for the much greater reduction in heating efficiency obtained at $k_\phi = -8\ \mathrm{m}^{-1}$.

Another possible channel for losing significant RF power at longer wavelengths is through preferred propagation of fast waves in the edge of the plasma where collisions and sheaths can cause significant damping of the waves. The cold plasma propagation characteristics for fast waves at $B = 2.82$ kG, the total magnetic field in front of the antenna Faraday shield for the $B_\phi = 4.5$ kG case, are given in Fig. 1, showing the strong dependence of propagation perpendicular to the equilibrium magnetic field on electron density and especially on wavelength.[13] In particular, for a given $k_\parallel$, if the edge density is too low, the wave is "cut off" and does not propagate in the direction perpendicular to the equilibrium magnetic field. In this case, the wave will "evanesce" into the plasma until it reaches a point where the local density is high enough for the wave to propagate. The density for onset of perpendicular propagation is approximately proportional to

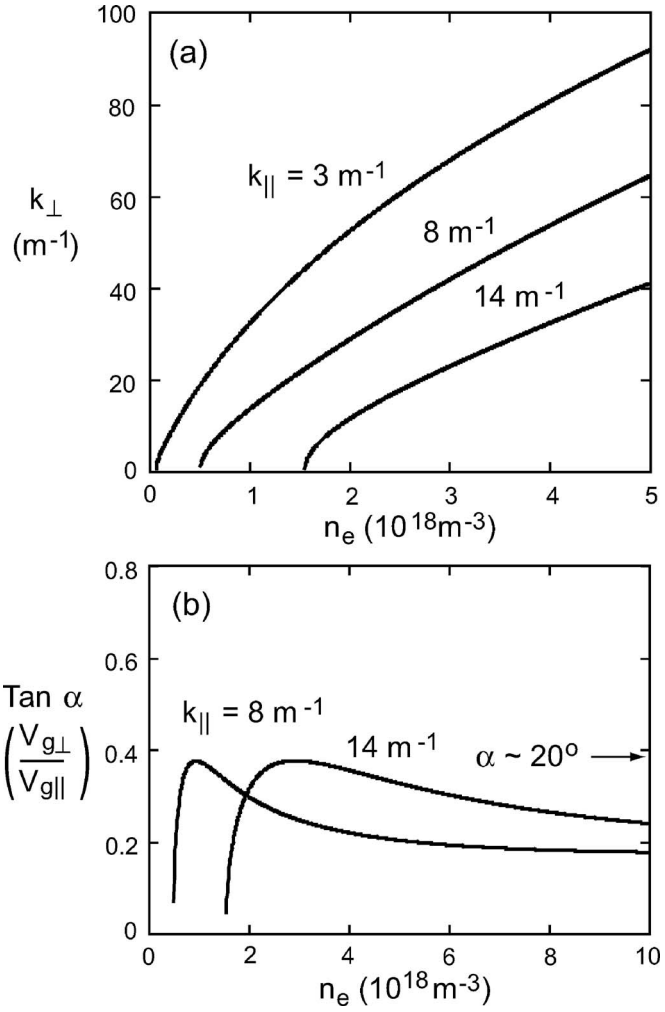

FIG. 1. High harmonic fast wave propagation characteristics for total magnetic field $B = 2.82$ kG at the antenna location on NSTX [toroidal field $B_\phi(R_o) = 4.5$ kG, plasma current $I_P = 0.6$ MA]. (a) Perpendicular wavenumber $k_\perp$ vs density for parallel wavenumbers $k_\parallel = 3\ \mathrm{m}^{-1}$, $8\ \mathrm{m}^{-1}$, and $14\ \mathrm{m}^{-1}$. (b) The tangent of the propagation angle α relative to the direction of B vs density. The onset density is $\propto B * k_\parallel^2/\omega$ and $\alpha < 20°$.

$B \times k_\parallel^2/\omega$ and, as indicated, the onset density for $k_\parallel = 8\ \mathrm{m}^{-1}$ is only $\sim 0.5 \times 10^{18}\ \mathrm{m}^{-3}$, compared to $\sim 1.6 \times 10^{18}\ \mathrm{m}^{-3}$ for $k_\parallel = 14\ \mathrm{m}^{-1}$ [Fig. 1(a)]. Thus, the propagation region in the longer wavelength case extends closer to the antenna/wall, in contrast to the shorter wavelength case. Furthermore, the perpendicular group velocity approaches zero near onset [Fig. 1(b)] so that the longer wavelength waves can be inhibited from entering the plasma even further if the density profile does not change much in the vicinity of the antenna.

In Sec. II A of this paper, results obtained at higher magnetic field, i.e., $B_\phi = 5.5$ kG,[14] for which the onset density is somewhat higher and the edge density gradient should be somewhat steeper, are presented to determine if the fast wave propagation in the plasma edge could contribute to the enhanced loss observed at $k_\phi = -8\ \mathrm{m}^{-1}$. In addition, the field dependence of PDI heating is evaluated to help separate the two loss channels. In Sec. II B, results from an expanded antenna phase (wavelength) scan are presented to show the constancy of heating efficiency for the wavelengths equal to or shorter than that for $k_\phi = -8\ \mathrm{m}^{-1}$ and the decrease in effi-

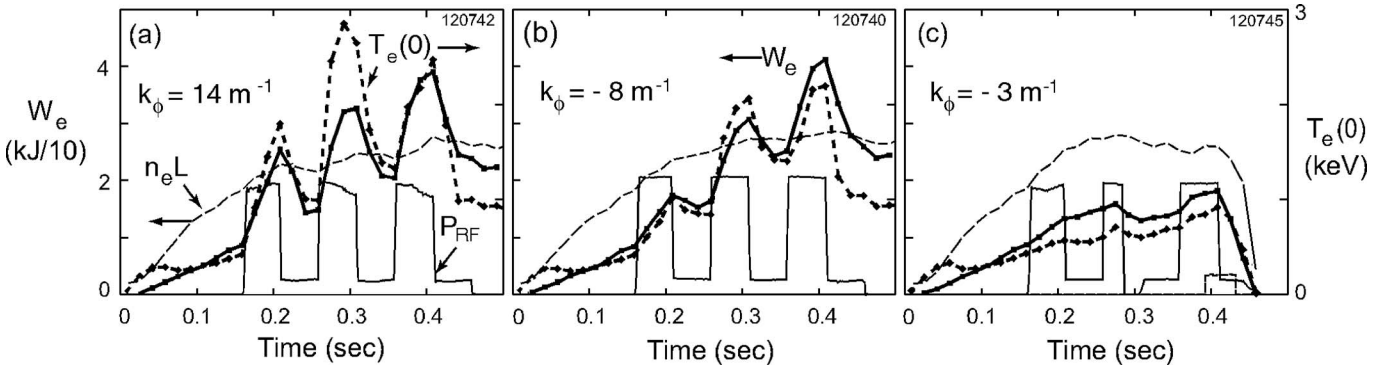

FIG. 2. Central electron temperature $T_e(0)$ and stored electron energy W_e vs time with RF power modulation for toroidal wavenumbers k_ϕ equal to (a) 14 m^{-1}, (b) −8 m^{-1}, and (c) −3 m^{-1}. [B_ϕ=5.5 kG, I_p=0.72 MA, P_{RF}=2 MW, and helium plasma.] Line average density is also shown for comparison between the shots (n_eL is in units of 10^{19} m^{-2} on the left scale).

ciency for wavelengths longer than that for k_ϕ=−8 m^{-1}. The competition between core damping and surface damping at k_ϕ=−3 m^{-1}, for which the wavelength is the longest, is also studied. The implications of NSTX HHFW surface wave loss for the low ion cyclotron harmonic regime, relevant to ITER, are discussed in Sec. II C. Finally, in Sec. III the first motional Stark effect[15] (MSE) measurements of HHFW CD effects on pitch angle and the estimated RF driven current are presented. The current predictions obtained with the full wave TORIC[16] and AORSA[17] codes are also presented for comparison.

II. HEATING EFFICIENCY AT HIGHER MAGNETIC FIELD

A. Improvement in heating efficiency for k_ϕ=−8 m^{-1} (cocurrent drive phase, −90°)

As shown in Fig. 2,[14] there is a dramatic improvement in heating with k_ϕ=−8 m^{-1} at B_ϕ=5.5 kG (I_P=720 kA) relative to the B_ϕ=4.5 kG (I_P=600 kA) case discussed previously in Ref. 10. The central temperature for k_ϕ=−8 m^{-1} for the third RF power pulse is close to that for k_ϕ=14 m^{-1}, and the corresponding line density is somewhat higher. The calculated values of W_e show the levels of heating at k_ϕ=−8 m^{-1} are now quite comparable to those at k_ϕ =14 m^{-1} for the last two RF pulses. However, for the first RF pulse of Fig. 2, the heating for the k_ϕ=−8 m^{-1} case is only about half that obtained at k_ϕ=14 m^{-1}.

To quantify the heating improvement obtained at k_ϕ=−8 m^{-1} by increasing B_ϕ, the electron stored energy obtained for 5.5 kG is compared to that obtained at B_ϕ =4.5 kG in Fig. 3. There is a factor of ~2 increase in ΔW_e at the higher B_ϕ for the third RF pulse over the same time interval in Fig. 3 (the RF pulse length has been increased from 33 to 50 ms at the higher B_ϕ). Furthermore, the exponential fits to the W_e data (see Fig. 3) show that the electron heating efficiency for the third RF pulse has been doubled at B_ϕ=5.5 kG to ~40%, compared to ~22% at B_ϕ=4.5 kG. Similarly, the total heating efficiency has been increased to ~65%, compared with ~44%.

In order to determine if the onset density for k_ϕ=−8 m^{-1} has moved away from the antenna for the higher magnetic field operation for the last two RF pulses, but not for the first RF pulse, the electron density at a radial location 2 cm in front of the antenna Faraday shield is measured with the Thomson scattering system. The edge densities measured for the k_ϕ=−8 and 14 m^{-1} discharges of Fig. 2 are shown in Fig. 4(b) and compared to the corresponding W_e curves in Fig. 4(a). As indicated, the edge densities 2 cm away from the antenna are at or below the onset density for k_ϕ=−8 m^{-1} for the last two pulses, so that the waves do not propagate at that location. However, the edge density is well above the k_ϕ=−8 m^{-1} onset density for the first pulse, indicating that fast wave propagation at or near the antenna/wall is responsible for the observed reduced heating efficiency. The edge density exceeds the onset density for k_ϕ=14 m^{-1} (2 cm in front of the antenna) only during the first part of the first RF pulse, appearing to force a slower rise in W_e during that time [Fig. 4(a)].

It is important to note that the core damping of the fast wave is a strong function of both $k_\parallel$ and B.[13] It is predicted

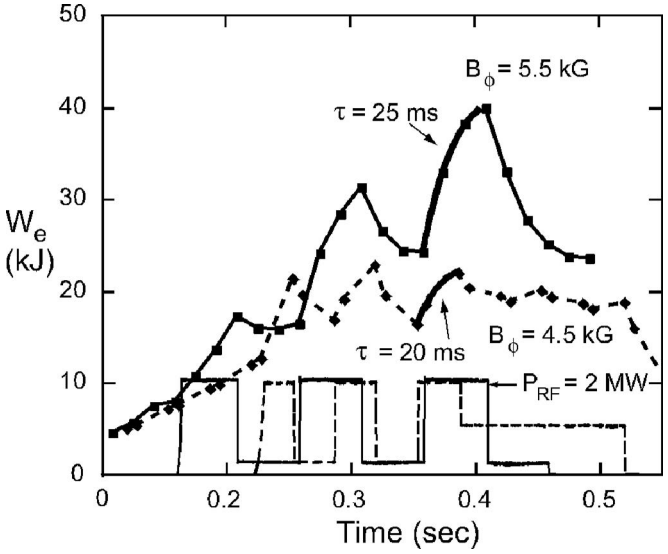

FIG. 3. Comparison of time plots of stored electron energy W_e obtained at B_ϕ=5.5 kG (solid curve) and B_ϕ=4.5 kG (dashed curve) for k_ϕ=8 m^{-1}. Exponential fits to the last RF pulses [Eq. (1)] give electron heating efficiencies of 40% and 22% for B_ϕ=5.5 kG and 4.5 kG, respectively. [Conditions for B_ϕ=5.5 kG are those of Fig. 2. Conditions for B_ϕ=4.5 kG are I_P =0.6 MA, P_{RF}=2 MW and helium (Ref. 10).]

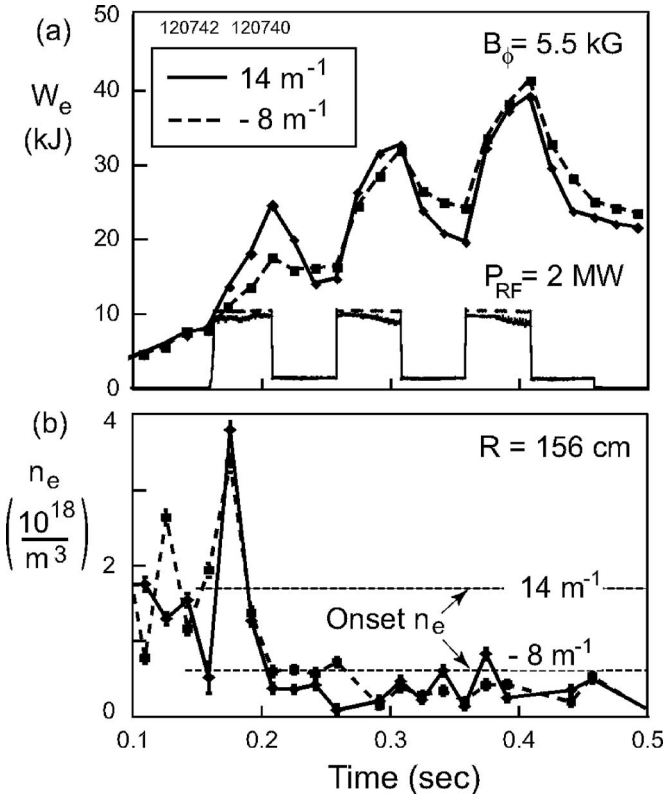

FIG. 4. (a) Time dependence of electron stored energy (W_e) with maximum modulated RF power of 2 MW, one with k_ϕ=14 m^{-1} (solid curve), and the other with k_ϕ=−8 m^{-1} (dashed curve). (b) Edge electron density (2 cm in front of Faraday shield) vs time. The onset density for k_ϕ=14 m^{-1} and k_ϕ =−8 m^{-1} perpendicular propagation is indicated by the horizontal dashed lines.

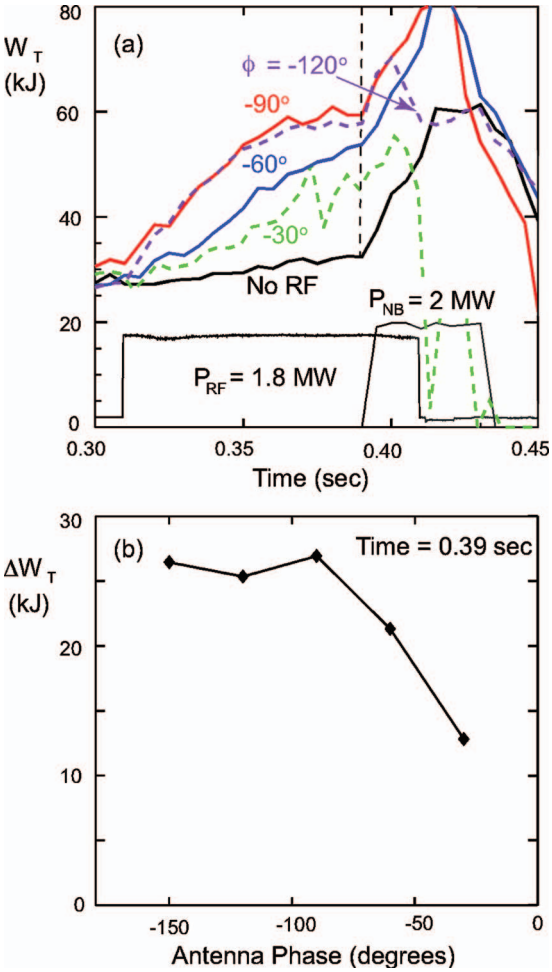

FIG. 5. (Color) (a) Time dependence of total stored energy (W_T) for a pulsed RF power of 1.8 MW vs the phase ϕ between antenna straps [ϕ=−90° corresponds to co-CD phasing (k_ϕ=−8 m^{-1})]. (b) Change in total stored energy (ΔW_T) at time=0.39 s {just prior to injection of the diagnostic neutral beam pulse [dashed vertical line in Fig. 5(a)]} showing the fall-off of heating at longer wavelengths, $|\phi|<90°$. B_ϕ=5.5 kG; I_p=0.6 MA, helium.

that the damping decrement $k_{\perp i}$ falls off rapidly with decreasing normalized wavenumber $n_\parallel = ck_\parallel/\omega$ being significantly above zero down to $n_\parallel \sim 5$ for NSTX-like conditions, and also decreases as B^{-3}. Therefore, the fact that heating efficiency improves substantially for the k_ϕ=−8 m^{-1} (toroidal mode number n_ϕ=12) case upon increasing the magnetic field from 4.5 to 5.5 kG, even though the damping decrement is predicted to be lowered by a factor of 0.55, again suggests that the surface losses are reduced substantially by moving the onset density away from the antenna/wall.

The possibility that a reduction in PDI losses at the higher field could account for the strongly improved heating efficiency at k_ϕ=−8 m^{-1} is not supported by the ERD spectroscopic measurements of edge ion heating.[12] It is found that the edge ion heating as indicated by the Gaussian fits to the energetic helium ion distributions is a very weak function of B_ϕ, in agreement with the predictions based on Eq. (11) of Ref. 9. In fact, the calculated PDI loss at B_ϕ=5.5 kG is comparable to that at B_ϕ=4.5 kG, whereas the overall loss decreased by ~21%. Furthermore, the PDI loss at k_ϕ=−3 m^{-1} is comparable to that at k_ϕ=−8 m^{-1}, whereas the overall loss at k_ϕ=−3 m^{-1} is much larger than that at k_ϕ=−8 m^{-1}, as clearly indicated in Fig. 2. Thus, perpendicular fast wave propagation very near to or at the antenna/wall is a leading candidate for explaining the enhancement of power loss with an increase in wavelength launched by the antenna.

B. Reduction of heating efficiency at longer wavelengths (k_ϕ<−8 m^{-1}, corresponding to phase <−90°)

The central electron heating and increase in W_e are very poor indeed for k_ϕ=−3 m^{-1} even at the higher field B_ϕ =5.5 kG (Fig. 2), and the propagating region still extends beyond the location of the antenna face for this case. In order to better quantify the effect of heating efficiency degradation with decreasing k_ϕ, an antenna phase scan has been made for nominally constant programmed discharge control parameters, such as I_P, B_ϕ, gas feed, and for discharges with minimal magnetohydrodynamic (MHD) activity. The resulting curves of total stored energy W_T versus time are shown in Fig. 5(a). The RF pulse shown gives good comparisons over an antenna strap-to-strap phase range of ϕ=−150° to ϕ=−30° (the ϕ=−150° curve is not shown for clarity). The RF pulse length has been increased to ~100 ms to allow W_T to attain near equilibrium values. It is found that at constant P_{RF}, the stored energy for an antenna phase of −90° (k_ϕ=−8 m^{-1}, co-CD phase) is indeed comparable to that for the higher phases (shorter wavelengths) at B_ϕ=5.5 kG, as

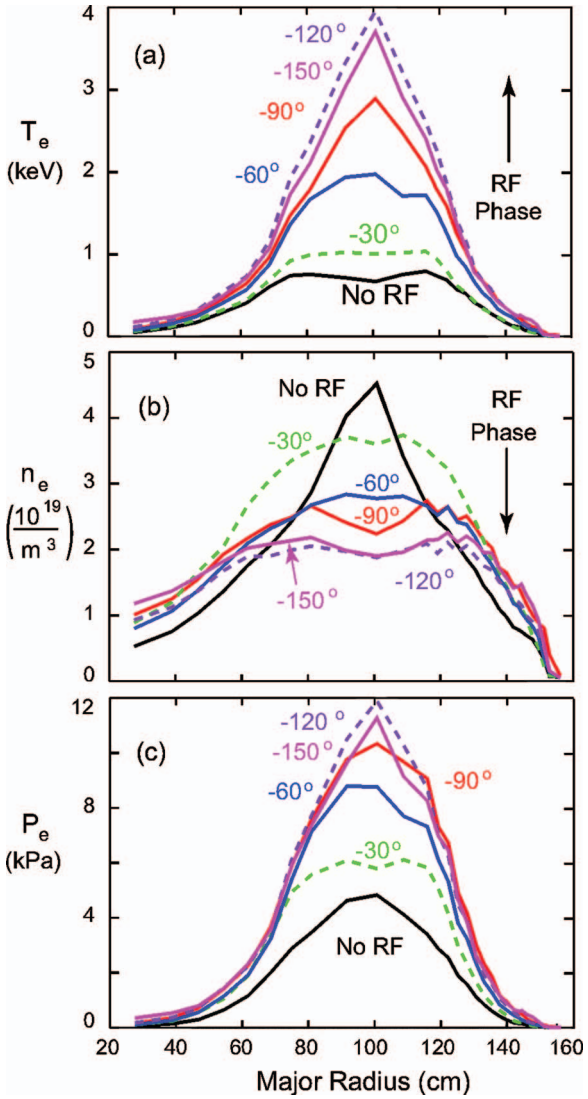

FIG. 6. (Color) Thomson scattering profiles vs antenna phase ϕ for time =0.375 s in Fig. 5 for (a) electron temperature $T_e(r)$, (b) electron density $n_e(r)$, and (c) electron pressure $p_e(r)$. (P_{RF}=1.8 MW for all antenna phases, ϕ.) $T_e(r)$ increases and $n_e(r)$ broadens and decreases with increasing $|\phi|$.

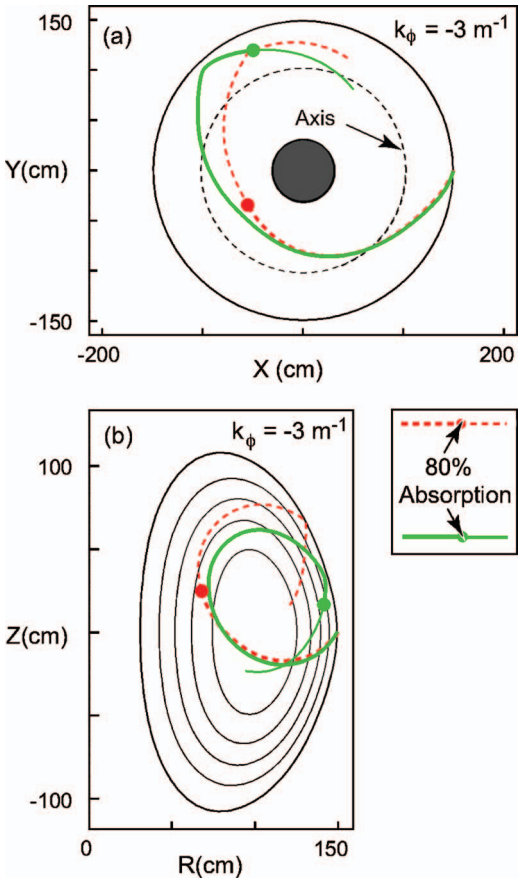

FIG. 7. (Color) k_ϕ=−3 m^{-1} ray tracing calculated by GENRAY, projected on to (a) the toroidal midplane and (b) a poloidal section. Calculations utilized temperature and density profiles from shot 123440 (solid green ray) and 123435 (dashed red ray). These shots were used in the experiment for k_ϕ =−3 m^{-1} (−30° phase) launch and k_ϕ=−8 m^{-1} and (−90° phase) launch, respectively, of Fig. 5. The point on each ray where 80% of the RF power has been absorbed by the plasma is indicated by the colored dot.

found above for antenna phases of 180° (k_ϕ=14 m^{-1}) and −90° (k_ϕ=−8 m^{-1}) (Fig. 2). However, the heating efficiency degrades at the lower strap-to-strap phases of ϕ=−60° and ϕ=−30° (i.e., longer wavelengths), as indicated by the fall-off in ΔW_T in Fig. 5(b).

The reduction of ΔW_T at longer wavelengths suggests again that surface losses are higher with the density at the antenna/wall above the onset density in these cases. However, the change in stored energy ΔW_T produced at ϕ=−30° is about 1/2 that obtained for phases of ϕ=−90° and above, which is actually higher than expected from the electron heating observed on axis (see Fig. 2). The explanation for the higher energy increment appears to be that there is a broadening and elevation of the density profile for the ϕ=−30° case relative to those for the higher phases, as indicated by the Thomson scattering profiles shown in Fig. 6, taken at t=0.375 s (prior to applying the diagnostic neutral beam pulse). The profiles indeed evolve with phase: $T_e(r)$ increases, $n_e(r)$ decreases on axis and broadens, and $P_e(r)$ increases on axis and broadens as phase is increased from ϕ=−30° to ϕ=−150°. This result suggests the RF power may be affecting transport, producing high core temperature and broad density profiles when core damping is strong and surface damping is weak, and producing low core temperature and more peaked density profiles (closer to the ohmic core level) when the core damping is weak and the surface damping is strong.

The surface damping is apparently enhanced for the ϕ =−30° case, since the fast waves are riding on the antenna and at or near the wall. However, the core damping is expected to be smaller as well since the single pass damping in the plasma core is also a strong function of $k_\parallel$.[13] If the single pass damping is relatively small, permitting multiple transits of the wave through the plasma, the core pressure buildup should be slower for the lower T_e levels, since both core heating decreases and surface losses increase with decreasing $k_\parallel$. In order to assess the competition between core damping and surface damping, the number of passes of the fast wave rays through the plasma must be modeled using the actual plasma profiles.

Ray tracing results calculated with the GENRAY code[18] for the damping of the ray with k_ϕ=−3 m^{-1} (ϕ=−30°) are

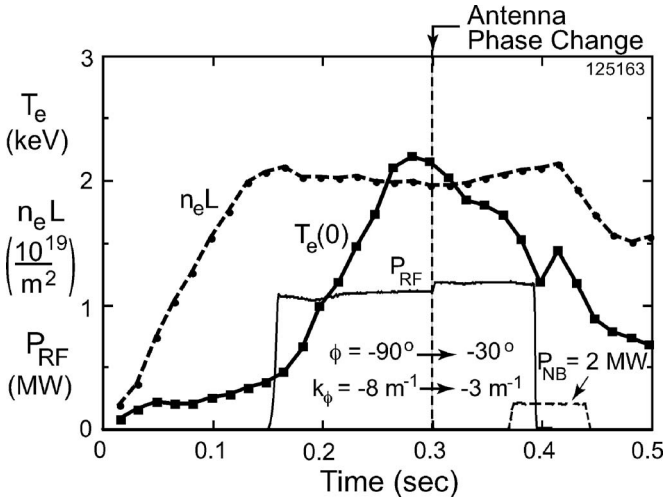

FIG. 8. Decay of central electron temperature $T_e(0)$ for antenna phase of $\phi=-30°$ ($k_\phi=-3$ m^{-1}) after preheating the electrons to $T_e(0)=2.2$ keV at $\phi=-90°$ ($k_\phi=-8$ m^{-1}) to provide single pass damping of the $k_\phi=-3$ m^{-1} wave (Fig. 7). $B_\phi=5.5$ kG; $I_P=0.6$ MA, helium plasma.

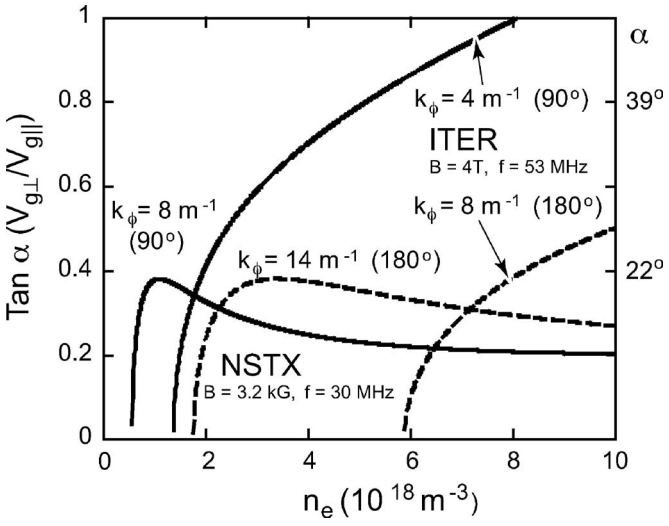

FIG. 9. Onset density and angle of ray propagation comparison between NSTX and ITER. The ITER ion cyclotron antenna concept dimensions give toroidal wavenumber k_ϕ values of 4 and 8 m^{-1} for 90° and 180° strap-to-strap phasing, respectively, for a magnetic field at the antenna of $B=4$ T and an operating frequency of $f=53$ MHz.

shown in Fig. 7, using the $T_e(r)$ and $n_e(r)$ profiles for both the $\phi=-30°$ and $\phi=-90°$ discharges from Fig. 6. For the $\phi=-30°$ profile conditions, the ray damps by ~70% in one pass through the plasma. This high first pass damping is a result of the ray path passing through the relatively high β core of the plasma without reaching the inner colder region of the plasma near the inner vessel wall. With the higher core temperature found for the $\phi=-90°$ profile conditions, it is predicted that the $\phi=-30°$ launched wave would have damped by 80% in only ~1/2 pass through the plasma (Fig. 7). Thus, it appears that the surface losses for the −30° case at $B_\phi=5.5$ kG occur primarily when the wave first enters the plasma at the antenna location.

To test the hypothesis that surface damping is indeed dominating the first pass damping, core electron heating has been measured at $\phi=-30°$ phasing for a higher temperature target plasma preheated by RF at $\phi=-90°$, as shown in Fig. 8. After the phase change to $\phi=-30°$, there is a gradual fall-off of $T_e(0)$ and a slight rise in $n_e(0)$, indicating that even with essentially complete first pass damping, surface losses in the vicinity of the antenna are still too large for $T_e(0)$ to be maintained. In addition, the profiles of T_e and n_e appear to be beginning an evolution toward those that are normally supported with $\phi=-30°$ without preheating. For the earlier studies at a lower $B_\phi=4.5$ kG,[19] in which core electron heating at $\phi=-30°$ followed preheating at $\phi=-90°$, the fall-off time of $T_e(0)$ was much shorter: $T_e(0)$ dropped from 1.8 to 0.7 keV (near ohmic level) in only ~30 ms. This comparison indicates that the surface losses are significantly reduced for $\phi=-30°$ at the higher magnetic field, even though the onset density has not been completely separated from the antenna.

C. Implications of NSTX HHFW surface wave loss results for the low ion cyclotron harmonic regime: ITER

The enhanced surface losses observed when the density at the antenna or wall is at or above the onset density for perpendicular propagation could be important for the low harmonic ion cyclotron regimes as well. Although the waves propagate more directly into the plasma core in this case,[20] generally, the occurrence of propagating fast wave fields immediately at the antenna can still cause considerable power deposition on the antenna and adjacent surfaces. Notably, for 0° antenna strap-to-strap phasing on TFTR, for which the edge of the plasma touched the antenna Faraday screen, the surface fast waves severely heated the screen at moderate power levels, releasing high levels of screen coating materials into the plasma.[5] This could also be an important consideration for ITER. As shown in Fig. 9, the k_ϕ parameters for the ITER IC antenna[21] are relatively low (center-to-center strap separation is 0.385 m), so that for CD phasing (90°) at 53 MHz operation, the onset density for perpendicular propagation is $\sim 1.4\times10^{18}$ m^{-3}. It may be difficult to stay below this edge density in ITER, especially if increasing the density in the scrape-off layer is desired to raise the coupling resistance of the antenna to permit the planned 20 MW of RF power to be delivered to the plasma.[22]

III. INITIAL MSE MEASUREMENTS OF HHFW CURRENT DRIVE

The improved heating efficiency obtained for CD phasing $\phi=-90°$ ($k_\phi=-8$ m^{-1} in Fig. 3) provides a good target condition for beginning the study of HHFW CD on NSTX using the MSE diagnostic.[15] The MSE diagnostic has been developed especially for the low B field conditions of NSTX. It is used to make measurements of the pitch angle of the equilibrium magnetic field, from which the current density profile is obtained by applying fits to the MSE data using the LRDFIT equilibrium reconstruction code.[23] To enable these measurements, a diagnostic neutral beam (NB) blip is injected at a 90 kV injection voltage at the desired time of measurement. Profiles of pitch angle are then provided in a sequence of 10 ms time intervals during the blip. The 2 MW

of power of this "diagnostic" NB is comparable to the HHFW power level, and is found to perturb the plasma during the later time intervals. For the results reported here, the MSE values are used for the first 10 ms time slice when there is no evidence of instability or degradation of confinement. Normally, this means that a clear ramp is observed in the total stored energy from the start of NB injection (due to the neutral beam enhancement of ion stored energy). However, the stored electron energy is not significantly affected during the first 10 ms time interval, nor is MHD stability. Such conditions were obtained for the $\phi=-90°$, $\phi=-60°$, and the no-RF cases of the phase scan in Fig. 5. The MSE results for these three phases are shown in Fig. 10. The change in pitch angle in the central region of the plasma relative to the no-RF case is slight at $\phi=-60°$, but is much more pronounced at $-90°$. The curve at $-60°$ suggests possible heating and CD effects, but for $-90°$ phasing a clear indication of a core CD effect is evident.

It has proven difficult to adjust the LRDFIT equilibrium reconstruction curves to fit the MSE data in the core region of the plasma ($R \leqslant 1.2$ m). Therefore, estimates of the current density have been obtained directly from the MSE pitch angle measurements using the LRDFIT magnetic surfaces at the location of the MSE data points. The total currents inside the corresponding areas divided by the areas then give the toroidal current density curves shown in Fig. 10(b). A clear indication of RF CD is found for $\phi=-90°$, where the current density peaks for $\rho \equiv \mathrm{sqrt}(\psi_N) \leqslant 0.2$, where ψ_N is the normalized poloidal flux within a magnetic surface. The greater CD effect at $-90°$ is consistent with greater heating efficiency, i.e., more power is reaching the core (estimated to be up to $\sim$65% of the total RF power) and perhaps the more peaked spectrum launched for this case. Possible CD out to $\rho \sim 0.3$ is observed relative to the no-RF case. The measurements for larger ρ are not resolved for the RF power level and pulse length used in the experiment (note that the pulse time at maximum energy is relatively short in Fig. 5, i.e., $\sim$30 ms, and the equilibrium profile for j_{RF} is not attained). The integrated RF current for $\phi=-90°$ relative to the no-RF case is $\sim$15 kA, and relative to the $-60°$ case is $\sim$5 kA, inside $R=1.2$ m in Fig. 10(a).

Predictions for the RF driven current density, j_{RF}, obtained using the TORIC and AORSA full wave codes, are presented in Fig. 11 for the $-90°$ conditions of Fig. 10. The TORIC prediction is for a single toroidal mode of $n_\phi=-12$, whereas the AORSA prediction uses the full toroidal spectrum, modeled with 101 toroidal modes to include the finite width of the spectrum as well as both the co- and counterdirected waves. Both codes predict that j_{RF} peaks strongly toward the plasma axis, $\rho<0.2$, as found in Fig. 10, though the AORSA code gives a somewhat more narrow peak. The predicted integrated currents I_{RF} are $\sim$37 and 26 kA, respectively, for the TORIC and AORSA calculations (at $P_T=1.2$ MW for $\sim$65% heating efficiency). The strong reduction of j_{RF} due to electron trapping for the small aspect ratio NSTX plasma is shown in Fig. 11(a) (factor of $\sim$6 reduction in I_{RF}) and the integrated current for the full spectrum used in the AORSA simulation is shown in Fig. 11(b). For a single toroidal mode as used in the TORIC case, AORSA predicts

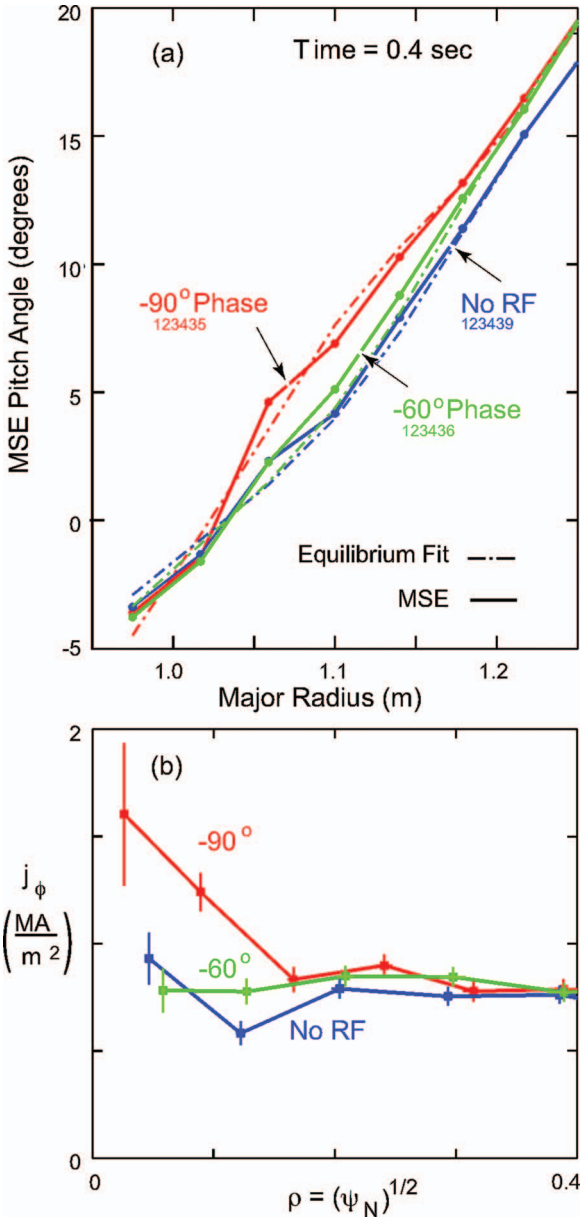

FIG. 10. (Color) (a) MSE pitch angle profiles vs major radius measured at the 0.400 s time slice for the antenna phase cases of $\phi=-90°$, $-60°$, and no-RF in Fig. 5. LRDFIT equilibrium reconstruction polynomial fits are also shown. (b) Toroidal current density vs the square root of normalized poloidal flux ρ obtained by fitting the measured pitch angles to the LRDFIT magnetic surfaces local to the measurements. The integrated current for $\phi=-90°$ relative to the no-RF case is $\sim$15 kA and relative to the $-60°$ case is $\sim$5 kA.

$I_{RF} \sim 34$ kA, in reasonable agreement with the TORIC value. The reduction of I_{RF} to $\sim$26 kA with 101 toroidal modes is due primarily to the inclusion of the counterdirected peak in the wave spectrum at $n_\phi \sim 38$. The predicted current for the 101 toroidal mode spectrum is $\sim$2 times the value indicated by the initial MSE measurements, which is reasonable agreement for the RF power and pulse length conditions used. Future CD studies at higher power will serve to benchmark the codes with each other and with the MSE measurements for the spherical torus regime.

The $|E_{RF}|$ field pattern produced with the 101 toroidal mode spectrum by the AORSA code is shown in Fig. 12. Note

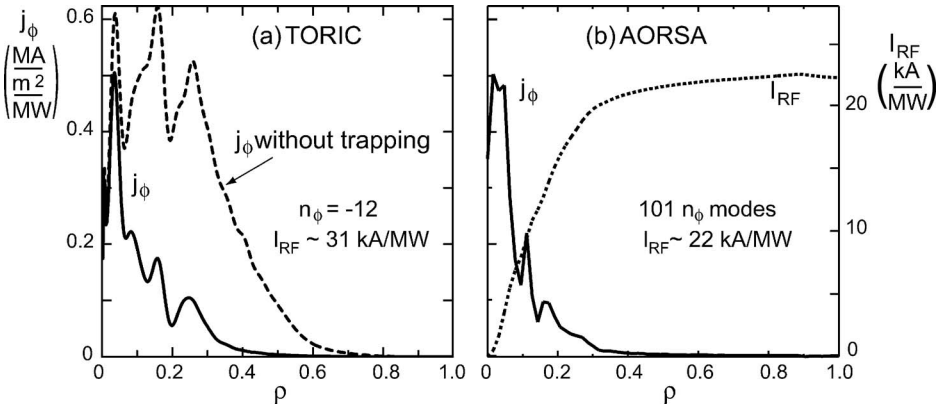

FIG. 11. The prediction of RF driven toroidal current density for the −90° antenna phasing case of Fig. 10 using (a) the TORIC two-dimensional full wave code (peak toroidal spectral ray k_ϕ=−8 m^{-1}, toroidal wavenumber n_ϕ =−12) and (b) the AORSA three-dimensional full wave code (101 toroidal wavenumbers). For a ~65% heating efficiency (P_T=1.2 MW), the integrated current is ~37 and ~26 kA for TORIC single mode and AORSA 101 mode cases, respectively. The current is decreased by a factor of ~6 from the no-trapping case.

that the waves propagate out from the antenna, penetrate into the core but without reaching the inner wall, and propagate around the plasma axis back to the outside wall. This wave pattern is consistent with the GENRAY ray results (Fig. 7; note that the B_ϕ and I_P directions in Fig. 12 are reversed relative to their directions in Fig. 7). The AORSA and TORIC codes are currently undergoing further development by the U.S. RF SciDAC project to include surface damping effects as well. In the future, NSTX can serve as a good platform for benchmarking these codes, since surface and core damping effects can be effectively separated for the relatively high β spherical torus plasmas.

IV. CONCLUSIONS

A dramatic increase in core heating efficiency at higher B_ϕ and lower edge density is observed on NSTX for CD phasing (ϕ=−90°). The associated losses are found to be a function of k_ϕ and edge density. These results strongly support the hypothesis that fast wave perpendicular propagation onset near the antenna or vessel wall is a primary cause for the reduction of heating efficiency at long wavelengths. This condition is especially important at very long wavelengths since the perpendicular onset density is $\propto B \times k_\parallel^2/\omega$. Thus, the reduced efficiency observed for in-phase fast wave operation generally,[3,4] with $k_\parallel$ approaching zero, would appear to be associated with this edge perpendicular propagation as well. The mechanisms by which the power is lost due to this surface propagation are not as yet resolved satisfactorily. Of course, sheath rectification at the antenna should be enhanced due to the higher near fields from the propagating modes there,[8] but additional processes must be considered as well. In particular, far field sheath effects should increase with wavelength. Higher fields and slower group velocities in the edge regions should enhance collisional damping, and it is possible that the RF reactive image currents induced in the plasma are brought close to the antenna or wall along with the perpendicular propagating region. This latter possibility could help explain the drastically increased Faraday shield heating observed with in-phase excitation on TFTR,[7] which appears to be too large to be explained simply by sheath rectification and convective cell properties alone.[24]

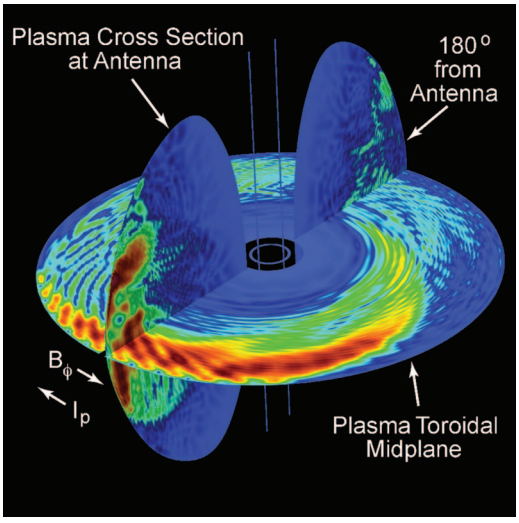

FIG. 12. (Color) AORSA three-dimensional $|E_{RF}|$ wave field amplitude (101 toroidal modes) for the −90° (k_ϕ=−8 m^{-1}) antenna phasing case of Fig. 10. Fields are indicated for the toroidal midplane and poloidal cross sections at the center of the antenna and 180° away.

Of course there is a competition between surface damping of the fast wave and its damping in the core as it passes through the plasma. Core damping decreases, and surface damping increases, with decreasing $k_\parallel$. GENRAY modeling shows that the wave is generally damped out in much less than one full pass through the NSTX plasma for the conditions of heating and CD (the ray propagates almost tangentially to the plasma axis in the core region) making it easier to minimize surface damping. Even at the very long wavelengths, for which the temperature is rather low, the primary ray damps by ~70% in one pass and thus interacts at the wall mainly in the vicinity of the antenna.

It is important to resolve all of the primary power loss mechanisms, since it is necessary to avoid significant surface losses in ITER. Due to the low wavenumber value for CD phasing on ITER, it is possible that the onset density will be exceeded at the blanket surface and near the antenna, and that the surface power losses could be significant, especially if the scrape-off layer density is enhanced in order to improve the coupling for the large gap foreseen between the antenna and the last closed field surface. NSTX results indicate that with and without gas puffing, careful tailoring of the density at the vessel tile surface and near the antenna to keep it below the onset density should be considered to limit edge power deposition to an acceptable level.

Initial measurements of HHFW CD have been made with MSE on NSTX. These are not easy measurements at the powers delivered to date (~1.2 MW into the core of the plasma). Nevertheless, indication of driven RF current density near the axis of the plasma is obtained for −90° CD phasing. TORIC and AORSA code estimates for j_{RF} are rather peaked within a $\rho \sim 0.2$, which is in reasonable agreement with the location of the j perturbation measured with MSE. The TORIC and AORSA predictions for total RF current are higher than the apparent driven current deduced from the MSE measurements (37 kA from TORIC and 26 kA from AORSA, compared with a maximum MSE value of ~15 kA). It would appear that the RF power was not applied long enough to reach equilibrium CD. Furthermore, the back EMF from the inductive drive could affect the results as well. However, it is clear from these initial CD results that the current driven is rather small for the small aspect ratio regime of NSTX for which electron trapping strongly reduces the CD. Considerably more RF power and longer RF pulses are needed to enhance the CD to a level to where more definitive measurements can be made. In addition, further modeling with the advanced RF codes being developed under the U.S. RF SciDAC program is needed to both determine the best conditions on NSTX for enhancing heating and CD while avoiding surface losses, and for benchmarking the codes for future applications generally.

ACKNOWLEDGMENTS

The authors appreciate the support given this work by Dr. Masayuki Ono and Dr. Jonathan Menard, the NSTX Team, and the machine, RF, and neutral beam operations groups.

This work is supported by DOE Contract No. DE-AC02-76CH03073.

[1] M. Ono, M. G. Bell, R. E. Bell *et al.*, Nucl. Fusion **41**, 1435 (2001).
[2] P. M. Ryan, A. L. Rosenberg, D. W. Swain *et al.*, *Plasma Physics and Controlled Fusion Research 2002*, Lyon (IAEA, Vienna, 2003), EX/P2-13.
[3] J. Jacquinot, H. Altmann, R. J. Anderson *et al.*, *Plasma Physics and Controlled Fusion Research 1986*, Kyoto (IAEA, Vienna, 1987), Vol. 1, p. 449.
[4] J. R. Wilson, M. G. Bell, A. Cavallo *et al.*, *Plasma Physics and Controlled Fusion Research 1988*, Nice (IAEA, Vienna, 1989) Vol. 1, p. 691.
[5] J. Stevens, C. Bush, P. Colestock *et al.*, AIP Conf. Proc. **190**, 342 (1989).
[6] M. Bures, J. Jacquinot, K. Lawson *et al.*, Plasma Phys. Controlled Fusion **33**, 937 (1991).
[7] J. Hosea, P. Bonanos, P. Colestock *et al.*, AIP Conf. Proc. **190**, 278 (1989).
[8] D. A. D'Ippolito, J. R. Myra, J. H. Rogers *et al.*, Nucl. Fusion **38**, 1543 (1998).
[9] J. R. Wilson, S. Bernabei, T. Biewer *et al.*, AIP Conf. Proc. **787**, 66 (2005).
[10] J. Hosea, S. Bernabei, T. Biewer *et al.*, AIP Conf. Proc. **787**, 82 (2005).
[11] S. A. Sabbagh, S. M. Kaye, J. Menard *et al.*, Nucl. Fusion **41**, 1601 (2001).
[12] T. M. Biewer, R. E. Bell, S. J. Diem, C. K. Phillips, J. R. Wilson, and P. M. Ryan, Phys. Plasmas **12**, 056108 (2005).
[13] M. Ono, Phys. Plasmas **2**, 4075 (1995).
[14] J. Hosea, R. Bell, S. Bernabei *et al.*, AIP Conf. Proc. **933**, 107 (2007).
[15] F. M. Levinton, H. Yuh, M. G. Bell *et al.*, Phys. Plasmas **14**, 056119 (2007).
[16] M. Brambilla, Plasma Phys. Controlled Fusion **44**, 2423 (2002).
[17] E. F. Jaeger, L. A. Berry, E. D'Azevedo, D. B. Batchelor, and M. D. Carter, Phys. Plasmas **8**, 1573 (2001).
[18] A. P. Smirnov and R. W. Harvey, Bull. Am. Phys. Soc. **40**, 1837 (1995).
[19] P. Ryan, D. Swain, J. R. Wilson, S. Bernabei, T. Biewer, S. Diem, J. Hosea, B. LeBlanc, and C. K. Phillips, Bull. Am. Phys. Soc. **49**, 69 (2004).
[20] P. T. Bonoli, D. B. Batchelor, L. A. Berry *et al.*, AIP Conf. Proc. **933**, 435 (2007).
[21] D. W. Swain and R. H. Goulding, Fusion Eng. Des. **82**, 603 (2007).
[22] M. Nightingale (personal communication, 2007).
[23] J. Menard (private communication, 2007). The LRDFIT Grad–Shafranov equilibrium reconstruction code uses a L-R circuit equation model of the plasma, vessel, and passive plate currents to better constrain the equilibrium fits, and self-consistently incorporates constraints from magnetics, radial electric field corrected MSE, T_e isosurfaces, and density/pressure asymmetries from centrifugal effects in the equilibrium reconstructions.
[24] L. Colas, E. Faudot, S. Bremond *et al.*, AIP Conf. Proc. **787**, 150 (2005).